



HAL
open science

Methane seep carbonates yield clumped isotope signatures out of equilibrium with formation temperatures

S. J. Loyd, J. Sample, R. E. Tripathi, W. F. Defliese, K. Brooks, M. Hovland, M. Torres, J. Marlow, L. G. Hancock, R. Martin, et al.

► To cite this version:

S. J. Loyd, J. Sample, R. E. Tripathi, W. F. Defliese, K. Brooks, et al.. Methane seep carbonates yield clumped isotope signatures out of equilibrium with formation temperatures. *Nature Communications*, 2016, 7, pp.12274. 10.1038/ncomms12274 . hal-02566170

HAL Id: hal-02566170

<https://hal.science/hal-02566170>

Submitted on 21 Jan 2021

HAL is a multi-disciplinary open access archive for the deposit and dissemination of scientific research documents, whether they are published or not. The documents may come from teaching and research institutions in France or abroad, or from public or private research centers.

L'archive ouverte pluridisciplinaire **HAL**, est destinée au dépôt et à la diffusion de documents scientifiques de niveau recherche, publiés ou non, émanant des établissements d'enseignement et de recherche français ou étrangers, des laboratoires publics ou privés.



Distributed under a Creative Commons Attribution - NonCommercial 4.0 International License

ARTICLE

Received 24 Mar 2016 | Accepted 17 Jun 2016 | Published 22 Jul 2016

DOI: 10.1038/ncomms12274

OPEN

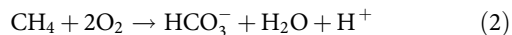
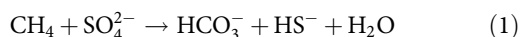
Methane seep carbonates yield clumped isotope signatures out of equilibrium with formation temperatures

S.J. Loyd^{1,2}, J. Sample³, R.E. Tripathi^{2,4,5}, W.F. Defliese², K. Brooks², M. Hovland⁶, M. Torres⁷, J. Marlow⁸, L.G. Hancock⁹, R. Martin¹⁰, T. Lyons⁹ & A.E. Tripathi^{2,4,5}

Methane cold seep systems typically exhibit extensive buildups of authigenic carbonate minerals, resulting from local increases in alkalinity driven by methane oxidation. Here, we demonstrate that modern seep authigenic carbonates exhibit anomalously low clumped isotope values (Δ_{47}), as much as $\sim 0.2\%$ lower than expected values. In modern seeps, this range of disequilibrium translates into apparent temperatures that are always warmer than ambient temperatures, by up to 50 °C. We examine various mechanisms that may induce disequilibrium behaviour in modern seep carbonates, and suggest that the observed values result from several factors including kinetic isotopic effects during methane oxidation, mixing of inorganic carbon pools, pH effects and rapid precipitation. Ancient seep carbonates studied here also exhibit potential disequilibrium signals. Ultimately, these findings indicate the predominance of disequilibrium clumped isotope behaviour in modern cold seep carbonates that must be considered when characterizing environmental conditions in both modern and ancient cold seep settings.

¹ Department of Geological Sciences, California State University, Fullerton, California 92831, USA. ² Department of Earth, Planetary and Space Sciences, University of California, Los Angeles, California 90095, USA. ³ School of Earth Sciences and Environmental Sustainability, Northern Arizona University, Flagstaff, Arizona 86001, USA. ⁴ Department of Atmospheric and Oceanic Sciences, Institute of the Environment and Sustainability, University of California, Los Angeles, California 90095, USA. ⁵ European Institute of Marine Sciences (IUEM), Université de Brest, UMR 6538/6539, Rue Dumont D'Urville, and IFREMER, Plouzané 29019, France. ⁶ Centre for Geobiology, University of Bergen, Bergen 5003, Norway. ⁷ College of Earth, Ocean, and Atmospheric Sciences, Oregon State University, Corvallis, Oregon 97331, USA. ⁸ Division of Geological and Planetary Sciences, California Institute of Technology, Pasadena, California 91125, USA. ⁹ Department of Earth Sciences, University of California, Riverside, California 92521, USA. ¹⁰ Department of Earth and Space Sciences/Burke Museum, University of Washington, Seattle, Washington 98195, USA. Correspondence and requests for materials should be addressed to S.J.L. (email: sloyd@fullerton.edu) or to A.E.T. (email: atripati@g.ucla.edu).

Methane cold seeps host diverse macro and microbiological communities^{1–5}. These ecosystems are driven by microbially mediated reactions involving methane-containing fluids advecting from depth⁶. As methane ascends it is primarily oxidized anaerobically by sulfate (termed the anaerobic oxidation of methane (AOM)), or aerobically in the presence of oxic seawater, as follows:



Both reactions produce bicarbonate, but only methane oxidation coupled with sulfate reduction increases alkalinity. The alkalinity production fostered by eq. 1 sustained by the relatively high concentration of sulfate in seawater promotes extensive carbonate (and sulfide) mineral production near methane seeps⁷. Complex microbial consortia facilitate sulfate reduction-coupled methane oxidation⁸ yielding extensive and generally rapid authigenic carbonate production in cold seep environments.

In an attempt to characterize the interactions in cold seep systems, both modern^{4,9–12} and ancient^{10,11,13–15} cold seep deposits have been studied extensively. Of particular importance is the characterization of ancient cold seep environmental conditions and their relationship to modern seep systems. However, due to the inherent issues associated with studies of past environments, characterization of ancient seeps hinges on the reliability of paleoproxies. A particularly useful parameter to quantify is precipitation temperature, as it dictates thermodynamic considerations such as abiotic versus biotic reaction times, and gas hydrate dynamics¹⁶. The newly emerging clumped isotope proxy has shown promise as a powerful geothermometer in the geosciences^{17–22}, yet the utility of clumped isotopes as an accurate geothermometer in cold seep carbonates has yet to be demonstrated.

Here, we demonstrate the occurrence of non-temperature dependent carbonate clumped isotope signatures in cold seep carbonates through analyses of modern precipitates forming under well-constrained conditions (that is, temperatures, pH, salinities and fluid $\delta^{18}\text{O}$ values). We compare modern systems with clumped isotope signatures in ancient seep carbonates, and discuss potential mechanisms to explain the observed disequilibrium values.

Results

Geologic context. Both modern and ancient cold seep carbonates are explored here. Modern samples originate from Hydrate Ridge, offshore Costa Rica, the Eel River Basin and the Norwegian Sea. Ancient samples originate from the Tepee Buttes Colorado (Cretaceous), the Panoche Hills California (Paleocene), the Quinault Formation (Mio-Pliocene), the Pysht Formation (Eocene) and the Lincoln Creek Formation (Oligocene; Fig. 1).

Modern cold seeps occur along continental margins and within large inland seas (for example, the Black and Mediterranean Seas)^{23,24}. These sites exhibit spatially and temporally variable delivery of subsurface methane, derived from sedimentary production (microbial or thermogenic), to relatively oxic marine waters²⁵. This methane is oxidized microbially either by reaction with dissolved oxygen or sulfate²⁶, as explained above. Photographs, photomicrographs and previously reported and new $\delta^{13}\text{C}$ and $\delta^{18}\text{O}$ values are provided in Figs 2–4, respectively.

Cold seep systems of Hydrate Ridge exhibit authigenic carbonate buildups in the form of chimneys, crusts, slabs, cements and concretions^{12,27–30}. These carbonate buildups are actively forming, and carbon-14 ages indicate that authigenesis has occurred within the last ~40 ka (ref. 30). Carbonate $\delta^{13}\text{C}$ ($\delta^{13}\text{C}_{\text{carb}}$) values are extremely negative and commonly extend to

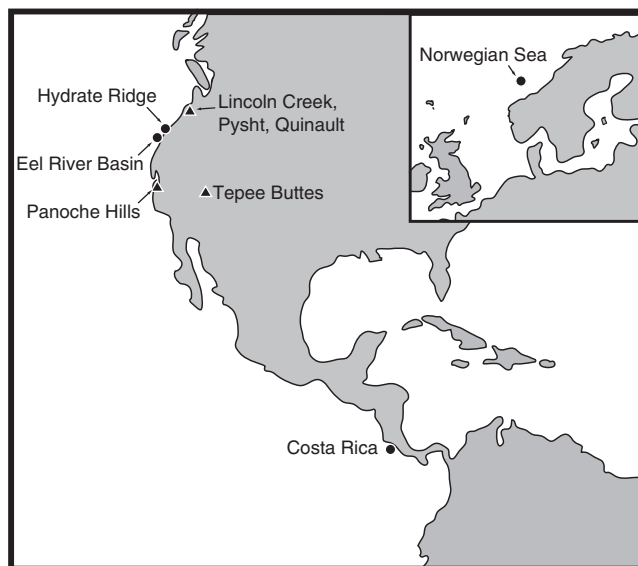


Figure 1 | Map of sample sites. Circles and triangles correspond to modern and ancient seep sites, respectively.

less than -30‰ (VPDB), indicative of a significant methane carbon source (Fig. 4). Carbonates consist of aragonite, calcite, high-magnesium calcite and dolomite primarily as micritic and acicular cements^{31–33} (Figs 2 and 3). Bottom water temperatures of Hydrate Ridge are $\sim 4\text{--}5\text{ °C}$ (ref. 12).

Authigenic carbonates (Figs 2 and 3) associated with cold seeps of the Eel River Basin occur primarily as irregular carbonate slabs, cements and concretions⁴. Erosion has exposed ancient carbonates, such that slabs commonly crop out on the seafloor despite formation in shallow sediments⁴. Authigenic carbonates are composed of magnesium calcite, aragonite and dolomite⁴. Aragonite and calcite $\delta^{13}\text{C}$ and $\delta^{18}\text{O}$ values do not overlap with dolomites but instead exhibit $\delta^{13}\text{C}$ and $\delta^{18}\text{O}$ values (Fig. 4) that range from -40 to -3.2‰ and $+3.2$ and $+5.8\text{‰}$, respectively. In contrast, dolomites express significantly ^{13}C -enriched values with $\delta^{13}\text{C}$ and $\delta^{18}\text{O}$ values ranging from $+5.0$ to $+15\text{‰}$ and $+6.1$ to $+8.9\text{‰}$, respectively⁴. The bottom water temperatures of Eel River Basin are $\sim 5\text{ °C}$ (ref. 4).

Cold seep sites off the coast of Costa Rica exhibit similar authigenic carbonate precipitates (Figs 2 and 3). These precipitates include concretions, carbonate ‘clasts’ and carbonate cemented muds³⁴. Larger buildups are oftentimes referred to as chemoherm carbonates due to the direct association with characteristic cold seep fossil assemblages^{9,32}. These chemoherm carbonates appear morphologically similar to slabs identified at the Hydrate Ridge and Eel River Basin localities. In addition, bottom water temperatures are $\sim 5\text{ °C}$, similar to Hydrate Ridge and Eel River Basin⁹.

The Norwegian Sea hosts cold seep systems yielding primarily aragonitic and calcitic carbonate buildups exposed in seafloor ‘pockmarks’³⁵. These buildups exhibit variable morphologies including crusts, ridges and blocky, tubular or irregular structures^{33,36}. Carbonate carbon and oxygen ($\delta^{18}\text{O}_{\text{carb}}$) isotope values are ~ -50 to -48‰ and $\sim +5$ to $+6\text{‰}$, respectively^{36,37} (Fig. 4), similar to values recognized at other modern cold seep sites. The bottom water temperatures are significantly colder than the other sites, ranging from ~ -1 to 1 °C (ref. 35).

In addition to modern seep carbonates, samples of Cretaceous to Oligocene seep carbonates from the western USA are explored here. These carbonates are inferred to have cold seep affinity due to depleted $\delta^{13}\text{C}$ values (below -30‰) and/or the presence of



Figure 2 | Photographs of cold seep carbonates. (a,b) Hydrate Ridge samples exhibiting light and dark primarily carbonate phases. (c,d) Costa Rica cold seep carbonate with micrite (MM1) and clotted micrite (MC1,2) sample sites indicated. (e,f) Eel River Basin cold seep dolomite samples exhibiting similar light and dark colour variation as Hydrate Ridge samples. Permanent marker cap is 5-cm long.

diagnostic cold seep fossils. The ancient seep carbonates from these localities exhibit similar fabrics to modern seeps including fibrous and finely crystalline micrites⁴. In addition to these, coarser-crystalline phases including sparry vug filling cements and various sparites occur. Typically, these spars express ¹⁸O-depleted and less ¹³C-depleted compositions, respectively, potentially indicative of formation during later diagenesis (Fig. 4). Ultimately, ancient seeps record a more complex paragenetic evolution than modern seep carbonates^{10,11,14,15,38}.

Modern cold seep carbonates. Carbonate carbon isotope compositions are generally very low, whereas oxygen isotope values are elevated (Fig. 4). Specifically, $\delta^{13}\text{C}_{\text{carb}}$ values range from -54.64 to -3.02‰ , -49.86 to -39.00‰ , $+13.97$ to $+15.95\text{‰}$, -52.01 to -50.82‰ for carbonates from Hydrate Ridge, Costa Rica, the Eel River Basin and the Norwegian Sea, respectively. Respective $\delta^{18}\text{O}_{\text{carb}}$ values range from $+3.11$ to $+7.76\text{‰}$, $+3.76$ to $+4.10\text{‰}$, $+7.26$ to $+7.34\text{‰}$ and $+4.72$ to $+5.42\text{‰}$ for carbonates from Hydrate Ridge, Costa Rica, the Eel River Basin and the Norwegian Sea. These isotope compositions are consistent with values observed in these and similar cold seep carbonates reported elsewhere^{4,11,12,27,37,39}.

Clumped isotope compositions (Fig. 5, Tables 1 and 2) overlap among all of the modern sample sites. In addition, clumped

isotope compositions of fibrous and micritic carbonates (the two most abundant phases recognized) do not exhibit crystal habit-related differences in Δ_{47} . The Δ_{47} values range from 0.620 – 0.679‰ , 0.639 – 0.677‰ , 0.706 – 0.740‰ and 0.705 – 0.783‰ for carbonates from Hydrate Ridge, Costa Rica, the Eel River Basin and the Norwegian Sea, respectively. Equilibrium values calculated for 1 and 5 °C bottom waters are 0.790 and 0.771‰ , respectively, using a steep slope calibration⁴⁰, and 0.768 and 0.753‰ , respectively, using a shallow slope calibration⁴¹. These calibrations were selected because both were generated partially or fully on the same instrument used for measuring the samples analysed for this study. The extent of disequilibrium (offset from expected equilibrium values) is $\sim +0.014$ to -0.134‰ in the most conservative scenario, and up to -0.008 to -0.152‰ (Table 3), yielding temperatures that are always warmer than ambient temperatures. These clumped isotope compositions translate to reconstructed temperatures ranging from 3–44 °C when a steep slope calibration is used⁴⁰. If a shallow slope calibration⁴¹ is used, the reconstructed temperatures range from -3 to 52 °C.

Ancient cold seep carbonates. Traditional $\delta^{13}\text{C}$ and $\delta^{18}\text{O}$ values show a wider range in ancient seep carbonates (Fig. 4). Carbon isotope values range from -45.21 to -14.31‰ , -30.08 to

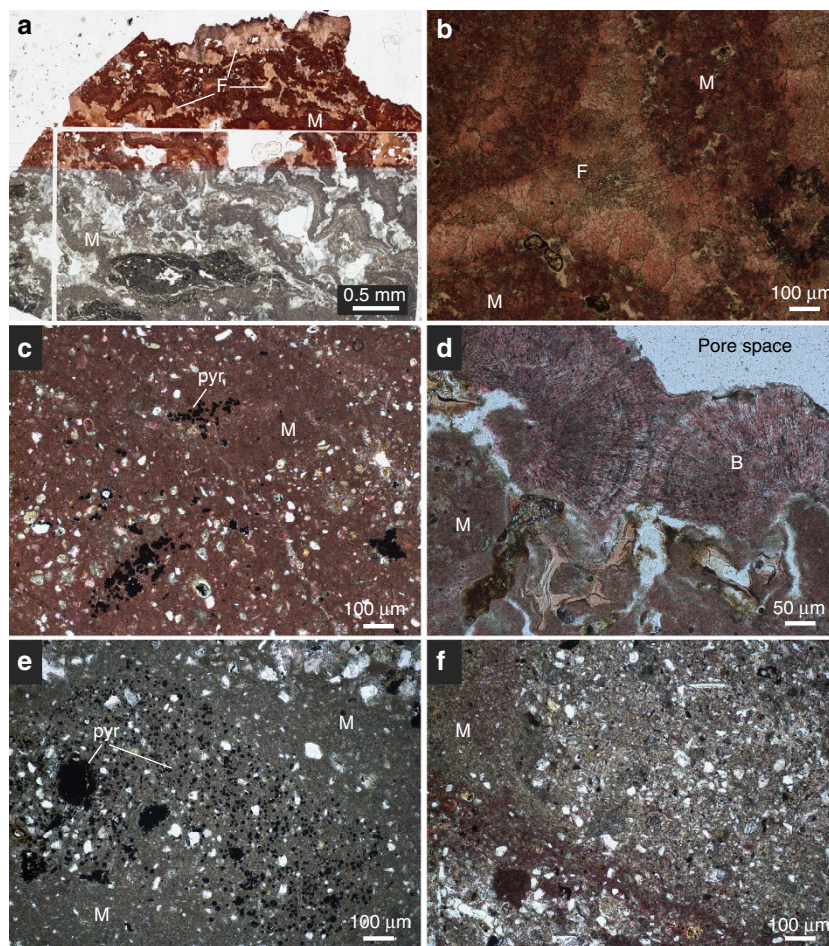


Figure 3 | Photomicrographs of cold seep carbonates. Red stain indicates calcium carbonate phases. Micritic (M), fibrous (F) and botryoidal (B) cements occur. (a,b) Hydrate Ridge samples composed of nearly pure calcium carbonate with a substantial fibrous component. (c) Costa Rica micritic carbonate with pyrite accumulations (pyr). (d) Micritic and botryoidal cold seep carbonate of Costa Rica, pale blue regions indicate pore space. White angular grains predominantly composed of quartz. (e,f) Eel River Basin largely micritic carbonates. The lack of stain in Eel River Basin sections indicates that these samples are predominantly composed of dolomite. Disseminated pyrite and pyrite accumulations occur in e. As in c, white grains in e and f composed of quartz.

− 6.05‰, − 19.33 to − 4.03‰ and − 34.99 to − 0.92‰ in cold seep carbonates of the Tepee Buttes, Quinault Formation, Pysht Formation and Panoche Hills, respectively (Table 2). Oxygen isotope compositions range from − 12.09 to − 0.30‰, − 8.32 to + 0.91‰, − 1.00 to + 1.53‰ and − 0.71 to + 2.25‰ in cold seep carbonates of the Tepee Buttes, Quinault Formation, Pysht Formation and Panoche Hills, respectively (Table 2). The Lincoln Creek Formation carbonate exhibits $\delta^{13}\text{C}_{\text{carb}}$ and $\delta^{18}\text{O}_{\text{carb}}$ values of − 15.16 and + 1.25‰, respectively (Table 2). These $\delta^{13}\text{C}_{\text{carb}}$ and $\delta^{18}\text{O}_{\text{carb}}$ values broadly overlap with those reported previously^{11,13,14,38,42,43} although some of the Tepee Buttes values are lower (Fig. 4).

Ancient cold seep carbonates exhibit clumped isotope compositions that range from those expressed by modern precipitates to significantly lower Δ_{47} values (Fig. 5; Table 2). Clumped isotope signatures from micritic, fibrous and sparry phases of the Tepee Buttes show no obvious crystallographic-specific distributions (that is, values generally overlap among phases). Tepee Buttes, Quinault Formation, Pysht Formation and Panoche Hills Δ_{47} values range from 0.377–0.521‰, 0.558–0.644‰, 0.611–0.631‰ and 0.649–0.705‰, respectively. A single sample from the Lincoln Creek Formation yielded a value of 0.623‰. Using the calibration by Tang *et al.*⁴¹, these

clumped isotope values translate to temperatures ranging from 107–286 °C, 42–83 °C, 47–56 °C, 19–40 °C and 46 °C, respectively (Supplementary Table 1). The calibration by Tripati *et al.*⁴⁰, calibration yields temperatures ranging from 81–169 °C, 37–66 °C, 41–47 °C, 20–35 °C and 40 °C, respectively (Supplementary Table 1).

Discussion

The $\delta^{13}\text{C}_{\text{carb}}$ values reported here from Hydrate Ridge, Costa Rica and the Norwegian Sea are consistent with carbonate formation from dissolved inorganic carbon generated via methane oxidation⁴. In contrast, the positive $\delta^{13}\text{C}_{\text{carb}}$ values of the Eel River Basin carbonates indicate formation in sediments experiencing microbial methane production⁴⁴. The $\delta^{18}\text{O}_{\text{carb}}$ values of cold seep carbonates are $\sim +3$ to $+5$ ‰ higher than those expected for carbonates precipitated in normal seawater with a $\delta^{18}\text{O}$ of ~ 0 ‰ (Fig. 4). These enriched oxygen isotope values may reflect gas hydrate (clathrate) dissolution at depth, the presence of which has been established at most of the study sites^{4,9,12,37}.

The clumped isotope values presented in this study are not in isotopic equilibrium with ambient temperatures of precipitation.

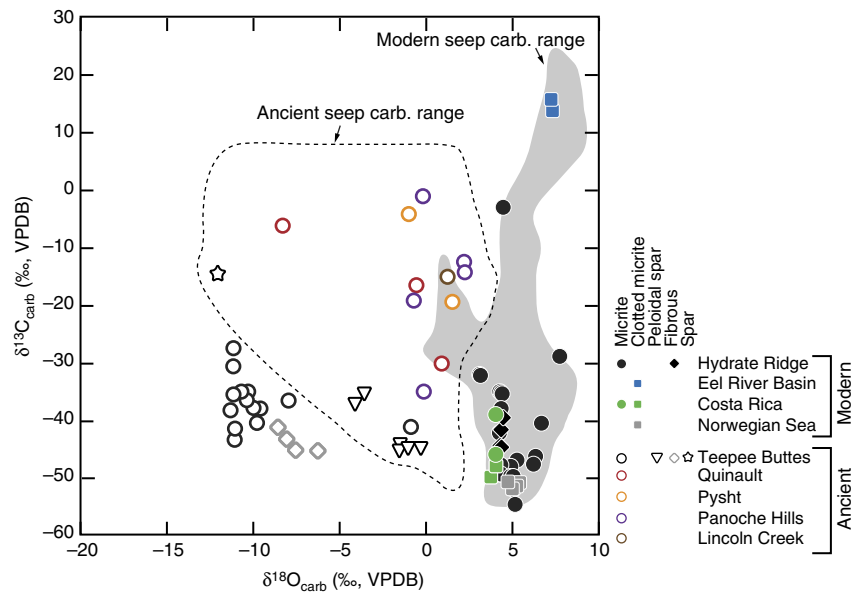


Figure 4 | Carbon and oxygen isotope values of modern and ancient cold seep carbonates. Ranges of previously reported values denoted by the grey envelope (modern^{4,11,12,32,37,39}) and dashed outline (ancient^{11,38,42}). Notice predominance of depleted $\delta^{13}\text{C}_{\text{carb}}$ values, typical of AOM carbonates. The enriched $\delta^{18}\text{O}_{\text{carb}}$ values expressed by modern cold seep carbonates has been interpreted to reflect incorporation of clathrate-dissolution-derived oxygen. Eel River Basin samples (micritic dolomites) exhibit positive $\delta^{13}\text{C}_{\text{carb}}$ values, indicative of a methanogenesis origin.

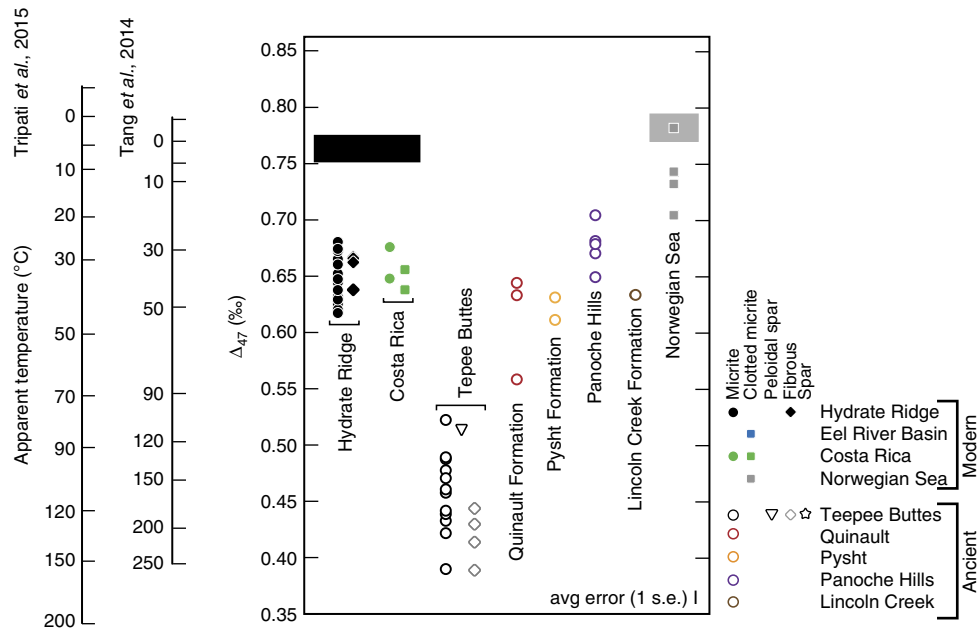


Figure 5 | Clumped isotope compositions and reconstructed temperatures. Also included are bottom water temperature ranges of the modern sites explored here. The grey envelope corresponds to Norwegian Sea and the black envelope corresponds to Hydrate Ridge and Costa Rica.

The sediment-water interface temperature at each site is $\sim 0\text{--}5^\circ\text{C}$ (refs 4,12,34,37). The Δ_{47} values are on the order of $\sim 0.1\text{‰}$ lower than expected for an equilibrium precipitate (Fig. 5, Table 3). This translates to significantly elevated carbonate formation temperatures (up to 52°C) compared with the ambient conditions and well beyond reasonable annual temperature variations of bottom waters. In some cases, authigenic carbonates associated with cold seeps have been postulated to grow after burial and then be exhumed by later sediment winnowing. Whereas this process may account for re-exposure

after shallow ($\ll 50\text{ m}$) burial, it seems very unlikely that winnowing would remove the 100s of metres of the sediment required to reach depths heated to $\sim 25^\circ\text{C}$ via burial. Of course, deep burial would be unnecessary if warm fluids were advecting from depth. Modern seep fluids are not hot enough to perturb the ambient bottom water temperatures, however, one could argue that fluid temperatures differed in the recent past. Ultimately, carbonate precipitation at elevated temperature is unlikely given the $\delta^{18}\text{O}_{\text{carb}}$ data, which are enriched compared with modern seawater and furthermore exhibit bulk isotope absolute values

Table 1 | Modern seep carbonate geochemical data

Sample	Phases	Modern Temp (°C)	$\delta^{13}\text{C}_{\text{carb}}$ (‰, VPDB)	stdv (‰)	$\delta^{18}\text{O}_{\text{carb}}$ (‰, VPDB)	s.d. (‰)	Δ_{47} (‰, ARF) AFF 0.000	Δ_{47} (‰, ARF) AFF 0.092	s.e. (‰)	s.d. (‰)	n
Hydrate Ridge											
Depth: 690 m; position: 44.6722°N, 125.1219°W											
2282-1c	Micrite	5	-52.07	0.010	5.10	0.024		0.632	0.013		1
2282-3	Micrite	5	-28.83	0.008	7.76	0.0215		0.666	0.0130		1
Depth: 630 m; position: 44.6694°N, 125.0480°W											
2284-1	Micrite	5	-47.57	0.008	6.27	0.013		0.661	0.012	0.028	2
2284-10	Micrite	5	-52.00	0.007	5.08	0.014		0.679	0.011		1
2284-2	Micrite	5	-46.98	0.005	5.28	0.009		0.663	0.012	0.034	2
2284-3	Micrite	5	-46.25	0.005	6.36	0.0149		0.643	0.0100		1
2284-4	Micrite	5	-48.07	0.007	4.95	0.011		0.649	0.014		1
2284-5	Micrite	5	-40.48	0.006	6.70	0.0191		0.672	0.0090		1
2284-6	Micrite	5	-54.64	0.005	5.16	0.016		0.659	0.013	0.039	2
2284-7	Micrite	5	-49.76	0.004	5.00	0.009		0.647	0.021	0.032	2
2284-8	Micrite	5	-3.02	0.001	4.44	0.0081		0.647	0.0294		1
2284-9	Micrite	5	-31.97	0.006	3.11	0.0121		0.636	0.0047		1
Depth: 800 m; position: 44.57°N, 125.15°W											
CS-1-B D1	Micrite	5	-49.53	0.003	4.35	0.007		0.662	0.010		1
CS-1-B D2	Micrite	5	-49.38	0.002	4.28	0.005		0.660	0.005		1
CS-1-B L2	Micrite	5	-35.26	0.003	4.34	0.007		0.620	0.009		1
CS-1-B-L1	Micrite	5	-37.92	0.002	4.38	0.009		0.663	0.006		1
cs-1-c d1	Micrite	5	-47.83	0.002	4.36	0.005		0.629	0.007		1
CS-1-C L1	Micrite	5	-35.81	0.004	4.51	0.004		0.650	0.013		1
CS-1-C L2	Micrite	5	-34.97	0.007	4.28	0.012		0.644	0.010		1
HR-4635 3364-L-1	Micrite	5	-42.16	0.006	4.26	0.016		0.652	0.021		1
CS-1-C A1	Fibrous cement	5	-44.63	0.003	4.41	0.007		0.667	0.007		1
CS-1-C A2	Fibrous cement	5	-44.36	0.003	4.32	0.007		0.638	0.013		1
CS-1-C-A3	Fibrous cement	5	-39.42	0.005	4.45	0.018		0.663	0.011		1
HR-4635 3364-A-1	Fibrous cement	5	-41.52	0.002	4.37	0.005		0.666	0.012		1
Eel River Basin											
Depth: 520 m; position: 40.812°N, 124.612°W											
ERB-4256-G4-A	Clotted micrite	5	13.97	0.005	7.34	0.016		0.740	0.010		1
ERB-4256-G4-B	Clotted micrite	5	15.95	0.005	7.26	0.013		0.706	0.008		1
Costa Rica											
Depth: 1,000 m; position: 8.93°N, 84.30°W											
CR-4501-L1-CM1	Clotted micrite	5	-49.86	0.003	3.76	0.013		0.639	0.011		1
CR-4501-L1 CM 2	Clotted micrite	5	-47.84	0.004	4.07	0.004		0.657	0.016		1
CR-4502-S3 MC 1	Micrite clast	5	-45.98	0.002	4.06	0.004		0.677	0.009		1
CR 4502-L2-MC2	Micrite clast	5	-39.00	0.002	4.10	0.007		0.649	0.009		1
Norwegian Sea											
Depth: 750 m; position: 64.67°N, 5.29°E											
H03 (90C)	Clotted micrite	1	-50.82	0.005	4.72	0.012		0.705	0.032		1
H03 (25C)	Clotted micrite	1	-50.97	0.004	5.42	0.009	0.744		0.021	0.051	2
H04 (90C)	Clotted micrite	1	-52.01	0.002	4.98	0.006		0.733	0.023		1
H04 (25C)	Clotted micrite	1	-51.57	0.881	5.24	0.395	0.783		0.017	0.018	2

consistent with equilibrium precipitation from ambient fluids. Therefore, we reject the possibility that the majority of these carbonates formed at temperatures consistent with the predictions based on the clumped isotope data.

Several factors are likely to be important in contributing to the observed clumped isotope disequilibrium signatures at methane seeps. We hypothesize that the AOM reaction (eqs. 1 and 2) produces a kinetic isotope signal in the clumped isotope composition of the generated DIC species (Fig. 6). Kinetic effects have been shown to result from CO_2 hydration and hydroxylation reactions (Fig. 6)^{17,45–47}, and dehydration/dehydroxylation reactions⁴⁵. Similar effects also occur in association with oxygen and carbon isotope partitioning among the gaseous and dissolved inorganic carbon phases⁴⁸. It is highly likely that rate-limiting

steps may occur during the methane oxidation process, which may be complex as AOM involves multiple intermediate reaction steps²⁵. We predict these rate-limiting steps may induce a large disequilibrium composition in product HCO_3^- or CO_3^{2-} , as with these other systems. Modern cold seep carbonate Δ_{47} values suggest that AOM leads to decreased Δ_{47} values. If the reactant methane results from gas hydrate dissolution, the AOM kinetic effects may be accompanied by $\delta^{18}\text{O}$ enrichment (Fig. 6b). Future work is needed to better constrain the magnitude and direction of offset in Δ_{47} of these effects on the composition of product DIC species.

The equilibrium clumped isotope composition of HCO_3^- and CO_3^{2-} are thought to differ from each other, and from carbonate minerals^{40,49}. Given that both pH and salinity affect

Table 2 | Ancient seep carbonate geochemical data.

Sample	Phases	$\delta^{13}\text{C}_{\text{carb}}$ (‰, VPDB)	stdv (‰)	$\delta^{18}\text{O}_{\text{carb}}$ (‰, VPDB)	s.d. (‰)	Δ_{47} (‰, ARF) AFF 0.092	s.e. (‰)	n
Tepee Buttes								
100-110	Micrite	-34.93	0.008	-10.31	0.0126	0.487	0.0175	1
130-140	Micrite	-37.75	0.007	-10.00	0.0114	0.432	0.0110	1
190-200	Micrite	-35.03	0.023	-10.64	0.3267	0.460	0.0185	1
20-30	Micrite	-36.40	0.004	-10.39	0.0056	0.457	0.0106	1
230-240	Micrite	-36.47	0.005	-7.97	0.0105	0.421	0.0090	1
250-260	Micrite	-35.41	0.002	-11.16	0.0087	0.389	0.0100	1
310-320	Micrite	-41.35	0.005	-11.07	0.0084	0.377	0.0138	1
320-2h	Micrite	-41.05	0.006	-0.89	0.009	0.521	0.011	1
360-370	Micrite	-43.28	0.007	-11.09	0.0168	0.441	0.0075	1
40-50	Micrite	-38.01	0.007	-9.60	0.0089	0.440	0.0115	1
65-70	Micrite	-38.16	0.004	-11.33	0.0113	0.477	0.0072	1
star 230-240	Micrite	-27.37	0.005	-11.10	0.0118	0.470	0.0138	1
teepee hrm 210-220	Micrite	-40.35	0.006	-9.80	0.007	0.438	0.012	1
teepee hrm 400-40	Micrite	-30.52	0.007	-11.17	0.0205	0.489	0.0122	1
100-110fc	Fibrous cement	-41.22	0.008	-8.60	0.0111	0.443	0.0094	1
190-200fc	Fibrous cement	-45.21	0.007	-7.57	0.0081	0.413	0.0153	1
210-220fc	Fibrous cement	-45.21	0.005	-6.28	0.0131	0.388	0.0167	1
460-470fc	Fibrous cement	-43.29	0.007	-8.09	0.0097	0.429	0.0085	1
711.5 VI S 2	Spar	-14.31		-12.09				1
320-2 PS	Peloidal sparite	-44.75		-0.30				1
704.5 1 PS	Peloidal sparite	-44.11		-1.50				1
711 WI PS	Peloidal sparite	-37.01		-4.12				1
711.5 VI PS 2	Peloidal sparite	-44.76		-1.04				1
711.5 VI PS1	Peloidal sparite	-45.16	0.008	-1.55	0.013	0.513	0.012	1
HRS 674.6 PS	Peloidal sparite	-35.16		-3.58				1
Quinault Fm								
Sample 1 Quin Fm	Micrite	-6.05	0.015	-8.32	0.012	0.558	0.014	1
Sample 9 Quin	Micrite	-30.08	0.002	0.91	0.007	0.633	0.014	1
Sample 11 Quin Fm	Micrite	-16.43	0.006	-0.56	0.014	0.644	0.012	1
Pysht Fm								
Sample 4 Pysht	Micrite	-19.33	0.004	1.53	0.011	0.631	0.009	1
Sample 5 Pysht	Micrite	-4.03	0.753	-1.00	3.050	0.611	0.020	1
Panoche Hills								
PTH 04	Micrite	-34.99	0.004	-0.13	0.009	0.680	0.011	1
PTH-07	Micrite	-14.17	0.003	2.25	0.011	0.705	0.012	1
PTH-08	Micrite	-12.53	0.007	2.25	0.015	0.682	0.010	1
PTH-18	Micrite	-19.11	0.007	-0.71	0.015	0.671	0.006	1
PTH-19	Micrite	-0.92	0.004	-0.18	0.017	0.649	0.012	1
Lincoln Creek Fm								
Sample 8 LC	Micrite	-15.16	0.006	1.25	0.012	0.634	0.008	1

DIC speciation, they can impart small but significant deviations in clumped isotope signatures of minerals (Fig. 6a)⁴⁹. Some cold seep carbonates may have formed in environments experiencing enhanced alkalinity production within relatively saline marine waters and/or fluids influenced by clathrate formation or dissociation⁵⁰. Theoretical modelling indicates that although the combined effects of salinity and pH affect clumped isotope values, the maximum expected differences in Δ_{47} are on the order of 0.035‰ over pH and salinity ranges of 5–14 and 0–50 parts per thousand, respectively⁴⁹. These ranges are beyond those observed in cold seep environments. Experimental data support a somewhat larger effect with maximum offsets of ~0.060‰ (ref. 40). We suggest that the effects of pH and salinity, although not sufficient enough to produce the full extent of clumped isotope anomalies observed here, may be a contributing factor given the range of fluid compositions at cold seeps.

Mixing of HCO_3^- or CO_3^{2-} from two different sources with distinct bulk ($\delta^{13}\text{C}$ and $\delta^{18}\text{O}$) and clumped isotope compositions does not necessarily yield a product reflecting simple linear mixing between end-members^{17,51,52}. Therefore it is feasible that mixing between DIC from seawater and DIC generated from AOM could induce anomalous clumped isotope signatures in the product carbonate minerals.

In addition, geochemically heterogeneous carbonates may yield clumped isotope compositions that do not reflect true precipitation temperatures of the mixture and/or individual end-members. Defliese *et al.*¹⁹ have demonstrated that mixing among carbonate phases with differing isotope compositions can produce inaccurate clumped isotope signatures and therefore have the potential to produce anomalous temperatures, such as those observed in cold seep carbonates. The degree to which the clumped isotope temperatures differ from linear mixing in a two-component system depends on the differing isotope

Table 3 | Degree of Δ_{47} offset from values expected from bottom water temperatures.

Sample	Phases	Modern Temperature (°C)	Δ_{47} (‰, ARF) AFF 0.000	Δ_{47} (‰, ARF) AFF 0.092	s.e. (‰)	s.d. (‰)	Δ_{47} disequilibrium	
							Tang et al. ⁴¹	Tripati et al. ⁴⁰
Hydrate Ridge								
2282-1c	Micrite	5		0.632	0.013		-0.121	-0.139
2282-3	Micrite	5		0.666	0.0130		-0.088	-0.105
2284-1	Micrite	5		0.661	0.012	0.028	-0.093	-0.111
2284-10	Micrite	5		0.679	0.011		-0.074	-0.092
2284-2	Micrite	5		0.663	0.012	0.034	-0.090	-0.108
2284-3	Micrite	5		0.643	0.0100		-0.110	-0.128
2284-4	Micrite	5		0.649	0.014		-0.105	-0.123
2284-5	Micrite	5		0.672	0.0090		-0.081	-0.099
2284-6	Micrite	5		0.659	0.013	0.039	-0.094	-0.112
2284-7	Micrite	5		0.647	0.021	0.032	-0.106	-0.124
2284-8	Micrite	5		0.647	0.0294		-0.107	-0.125
2284-9	Micrite	5		0.636	0.0047		-0.117	-0.135
CS-1-B D1	Micrite	5		0.662	0.010		-0.091	-0.109
CS-1-B D2	Micrite	5		0.660	0.005		-0.093	-0.111
CS-1-B L2	Micrite	5		0.620	0.009		-0.134	-0.152
CS-1-B-L1	Micrite	5		0.663	0.006		-0.090	-0.108
cs-1-c d1	Micrite	5		0.629	0.007		-0.124	-0.142
CS-1-C L1	Micrite	5		0.650	0.013		-0.103	-0.121
CS-1-C L2	Micrite	5		0.644	0.010		-0.109	-0.127
HR-4635 3364-L-1	Micrite	5		0.652	0.021		-0.101	-0.119
CS-1-C A1	Fibrous cement	5		0.667	0.007		-0.087	-0.105
CS-1-C A2	Fibrous cement	5		0.638	0.013		-0.115	-0.133
CS-1-C-A3	Fibrous cement	5		0.663	0.011		-0.090	-0.108
HR-4635 3364-A-1	Fibrous cement	5		0.666	0.012		-0.088	-0.106
Eel River Basin								
ERB-4256-G4-A	Clotted micrite	5		0.740	0.010		-0.013	-0.031
ERB-4256-G4-B	Clotted micrite	5		0.706	0.008		-0.048	-0.066
Costa Rica								
CR-4501-L1-CM1	Clotted micrite	5		0.639	0.011		-0.115	-0.133
CR-4501-L1 CM 2	Clotted micrite	5		0.657	0.016		-0.097	-0.114
CR-4502-S3 MC 1	Micrite clast	5		0.677	0.009		-0.077	-0.095
CR 4502-L2-MC2	Micrite clast	5		0.649	0.009		-0.104	-0.122
North Sea								
H03 (90C)	Clotted micrite	1		0.705	0.032		-0.063	-0.085
H03 (25C)	Clotted micrite	1	0.744		0.021	0.051	-0.024	-0.046
H04 (90C)	Clotted micrite	1		0.733	0.023		-0.035	-0.057
H04 (25C)	Clotted micrite	1	0.783		0.017	0.018	0.014	-0.008

compositions expressed by the two end-members. The offset is greatest when phases are most dissimilar, and mixing occurs in equal proportions (that is, a 50:50 mixture). Such mixing can produce clumped isotope compositions offset in either the positive or negative direction, yielding apparent low or high temperatures, respectively¹⁹. Modern and ancient cold seep carbonates commonly exhibit phase heterogeneity on 10–100 μm scales^{4,11,13–15} (Fig. 3). Current clumped isotope analytical protocols preclude sampling at this resolution, therefore cold seep carbonates may yield inaccurate temperatures as a result of phase mixing.

We address the possibility of mixing-related temperature anomalies by considering bulk isotope compositions and initial formation conditions of chemical species that contribute to modern cold seep carbonates. Cold seep carbonates commonly exhibit $\delta^{13}\text{C}_{\text{carb}}$ values that extend down to ~ -40 to -60‰ (Fig. 4), including those analysed here at the relatively large sample sizes required for clumped isotope quantification. We recognize the complexity of carbon cycling at the sulfate methane transition zone⁵³, however, as a first-order approximation, here

we assume that the $\delta^{13}\text{C}$ values represent near equal mixtures of DIC produced from AOM ($\delta^{13}\text{C}$ ranges from -60 to -100‰ ; in agreement with reported methane values^{34,37,54–56}) and the bulk seawater DIC pool ($\sim 0\text{‰}$). Some cold seep carbonates tend to exhibit $\delta^{18}\text{O}_{\text{carb}}$ values above normal marine precipitates ($\delta^{18}\text{O}_{\text{carb}}$ of $\sim +5\text{‰}$), consistent with precipitation from fluids associated with clathrate dissociation³². Maximum clumped isotope offsets are achieved when the end-members are most dissimilar¹⁹. In Fig. 7a we illustrate how cold seep $\delta^{13}\text{C}_{\text{carb}}$ values may relate to potential fractional contributions of methane-derived carbon (f_{methane}), by assuming a range of potential carbon isotope compositions of this methane (δ_{meth}) and a purely marine DIC end-member (with $\delta^{13}\text{C} = 0\text{‰}$). Many modern and ancient cold seep carbonates exhibit $\delta^{13}\text{C}_{\text{carb}}$ values that could reflect equal mixtures between these two end-members ($f_{\text{methane}} = 0.5$) and therefore have the potential to express maximum mixing-related clumped isotope composition offsets.

Two mixing models are explored here to potentially reconcile the Δ_{47} anomalies (Fig. 7). The first is relevant to a marine bottom water with a temperature of $\sim 5\text{°C}$, consistent with

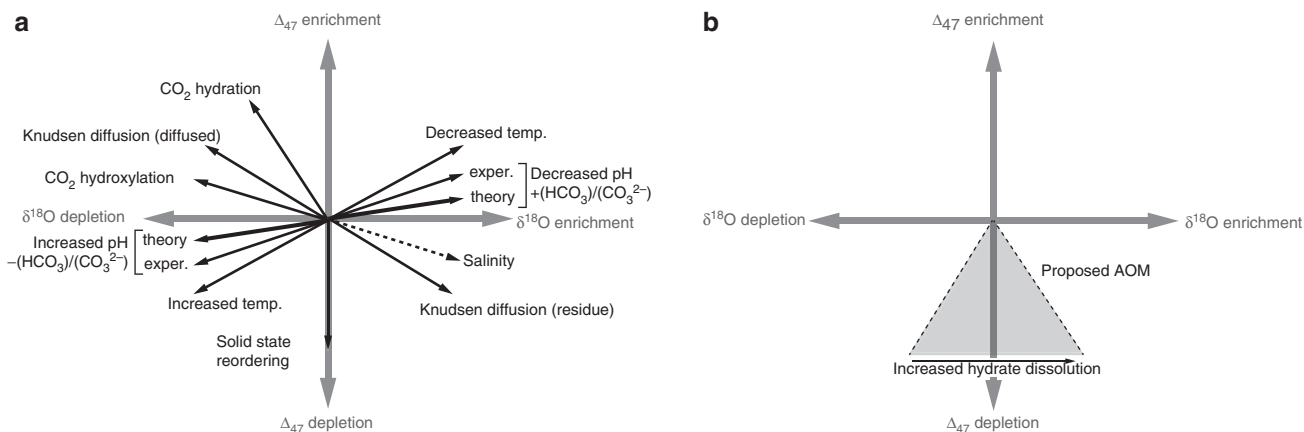


Figure 6 | Various controls on Δ_{47} values. (a) In addition to temperature²⁰, diffusion, salinity, pH and CO_2 hydration/hydroxylation reactions have been shown to influence the clumped isotope compositions of carbonates^{40,41,45,46,49,52}. CO_2 hydroxylation and hydration are pH sensitive, with hydroxylation favored at higher pH⁴⁶. Solid-state re-ordering may also impact carbonates, with increased rates at higher temperatures and greater potential for re-ordering in older rocks^{22,70}. Mixing has been shown to produce variability in multiple trajectories¹⁹. Increased salinity produces $\delta^{18}\text{O}$ enrichment and Δ_{47} depletion, however the specific slope can vary. (b) Hypothesized influences by AOM reactions and hydrate dissolution.

temperatures observed at Hydrate Ridge, Eel River Basin and Costa Rica. This temperature would yield a mineral Δ_{47} value of ~ 0.76 . The second simulates Norwegian Sea bottom waters, which exhibit temperatures of $\sim -1^\circ\text{C}$ from which an equilibrium-precipitated carbonate would exhibit a Δ_{47} value of ~ 0.77 . Mixing between more dissimilar end-members produces larger possible anomalies¹⁹. Here, the isotope compositions of the cold seep end-member include $\delta^{13}\text{C}$ values of -60 , -80 and -100‰ , a $\delta^{18}\text{O}$ value of $+5\text{‰}$ and Δ_{47} values of 0.71 and 0.72 . The isotope compositions of the marine end-member include a $\delta^{13}\text{C}$ value of 0‰ , a $\delta^{18}\text{O}$ value of 0‰ and Δ_{47} values of ~ 0.76 and 0.77 . Mixing models between the end-members described above generally do not produce the magnitude of observed temperature disequilibrium between cold seep carbonates and modern bottom waters (Fig. 7), even though mixing yields the maximum possible offset as constrained by environmental parameters.

AOM rates are variable in modern cold seep systems (Supplementary Fig. 1). Rates commonly correspond to the flux of methane from the deeper subsurface to sulfate-containing fluids. Vent-proximal, advection-dominated methane delivery is generally associated with higher AOM rates, whereas more peripheral, diffusive seepage is generally associated with lower AOM rates⁵⁷. As this reaction (eq. 1) produces alkalinity in equal molar proportions to the methane reactant, AOM is likely a first-order control on carbonate mineral authigenesis.

The anomalously low Δ_{47} values exhibited by modern seep carbonates may arise from rapid mineralization, which may allow them to retain an isotopic fingerprint of processes controlling solution disequilibrium, as well as surface kinetic processes. Quantitative models have shown that minerals forming rapidly will have a higher propensity to exhibit geochemical signatures out of equilibrium with the ambient environment⁵⁸, and recent observations have shown this can apply to clumped isotope signatures⁴⁰, although recent laboratory-based rapid precipitation experiments can yield equilibrium clumped isotope signatures⁵⁹. In cold seep settings, mineral precipitation rates are difficult to quantify, so that although there are many reports of AOM rates, authigenic carbonate precipitation rates are rarely available. Where carbonate precipitation and AOM rates have been quantified in the Nile Delta^{60,61} and Mediterranean Sea^{62,63} precipitation rates broadly overlap with AOM rates (see Supplementary Fig. 1). Therefore environments exhibiting

more rapid AOM rates may also exhibit more rapid carbonate precipitation rates and carbonates expressing more severe disequilibrium behaviour.

The above combination of factors likely explains the large disequilibrium signatures observed in modern seep carbonates. These same processes would be relevant in ancient seeps, and therefore it is reasonable to assume that ancient seeps also exhibit disequilibrium. The ancient seep carbonates measured here all show evidence for apparent temperatures that are too warm to reflect bottom waters. On the one hand, this is consistent with our explanation for modern seep disequilibrium, however, on the other hand, ancient deposits are generally composed of many distinct phases, some perhaps precipitated from warm, later diagenetic fluids^{11,13}.

We suggest that although modern samples record disequilibrium (that is, non-temperature dependent) Δ_{47} values, ancient samples may have experienced subsequent heating, solid-state re-ordering (Fig. 6) or both that may overwrite the signal and randomize ^{13}C - ^{18}O bonds from an initial ordering. Complex parageneses have been interpreted for ancient cold seep carbonate cement relationships^{11,14,15,38}. Thus in an ancient seep setting, extremely low Δ_{47} values could be recorded. In fact, it has been argued that Neoproterozoic Doushantuo carbonates exhibit low Δ_{47} values consistent with hydrothermal conditions⁵¹. However, based on our modern and ancient seep data, an alternative possibility is that the Doushantuo carbonates exhibited substantial disequilibrium Δ_{47} signatures on initial formation, and that subsequent processes (for example, solid-state re-ordering²²) have randomized the signatures from original values. Evidence to support this interpretation stems from our fossil seep carbonates of the Tepee Buttes, which show clumped isotope and $\delta^{18}\text{O}_{\text{carb}}$ values more similar to those of Doushantuo carbonates⁵¹ than modern seep carbonates.

In conclusion, modern cold seep carbonates exhibit Δ_{47} values ranging from 0.609 to 0.783‰ , significantly lower than equilibrium precipitation would yield. This disequilibrium translates into apparent formation temperatures of -3 up to 52°C , while modern, seep-proximal bottom waters are all $< 5^\circ\text{C}$. We hypothesize kinetic effects likely arise from a combination of processes, including AOM, DIC speciation effects and mixing, with the rapid precipitation rates in such settings leading to the high potential for incorporation of such kinetic isotope signals into carbonate minerals. In ancient cold seeps these same factors,

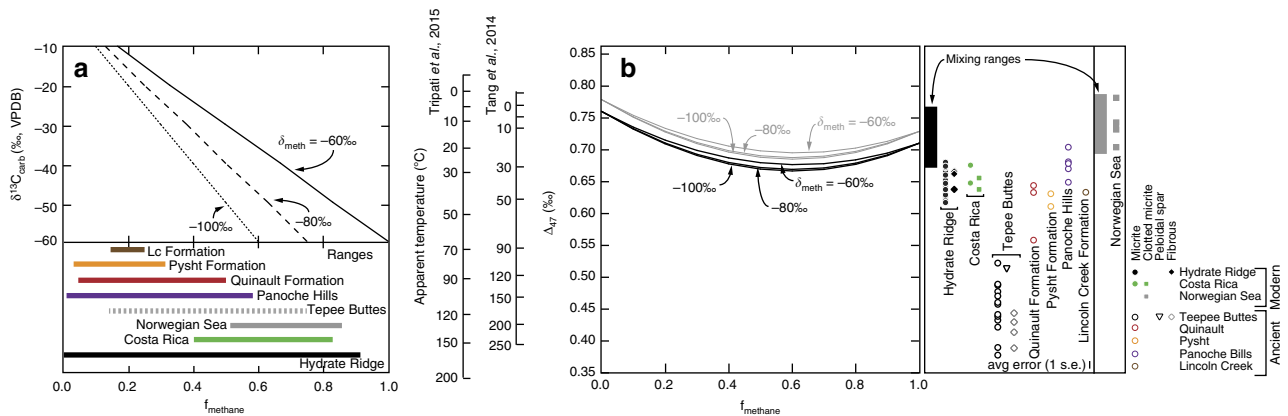


Figure 7 | Comparison of clumped isotope compositions with mixing-related temperature anomalies. (a) Diagram depicting the fractional contribution of methane-derived carbon (f_{methane}) based on $\delta^{13}\text{C}_{\text{carb}}$ values and a range of methane carbon isotope compositions (δ_{meth}). Here, f_{methane} is calculated assuming that carbon is derived from methane and seawater (with $\delta^{13}\text{C} = 0$). Ranges of f_{methane} arise from variable $\delta^{13}\text{C}_{\text{carb}}$ and hypothetical δ_{meth} values. Notice how modern and most ancient seep carbonate $\delta^{13}\text{C}_{\text{carb}}$ values overlap with those required for a 50:50 mixture (that is, $f_{\text{methane}} = 0.5$). (b) Results of mixing between two environmentally constrained end-members as calculated using the approach of Defliese *et al.*⁶⁵. Grey envelope and curves correspond to the potential range of values resulting from mixing in Norwegian Sea carbonates. Black envelope and curves correspond to all others. See text for information concerning end-member isotope compositions. Notice that mixing cannot account for the clumped isotope and temperature anomalies recorded in cold seep carbonates, both the Tripati *et al.*⁴⁰ and Tang *et al.*⁴¹ calibration-derived temperatures included. Note that dolomites of the Eel River Basin are not included in this diagram. This is because positive $\delta^{13}\text{C}_{\text{carb}}$ values indicate formation in the zone of methanogenesis and therefore potential mixing cannot be independently assessed as with the other samples.

in combination with burial diagenesis and/or solid-state reordering, can result in extremely low Δ_{47} values. Ultimately, our findings indicate that cold seep carbonates formed by AOM are susceptible to disequilibrium behaviour and therefore clumped isotopes cannot be used as a strict temperature proxy for the primary formation environment in modern or ancient seeps.

Methods

Sample collection. Carbonate samples were collected from modern cold seeps of Hydrate Ridge, off the western coast of Costa Rica, Eel River Basin and the Norwegian Sea (Fig. 1). Micritic and fibrous carbonate phases were microdrilled from these modern cold seep carbonates. Ancient cold seep carbonates were collected from outcrops of the Quinault, Pysht and Lincoln Creek Formations, the Tepee Buttes and the Panoche Hills (Fig. 1). In addition to micritic and fibrous phases, ancient carbonates also exhibit sparry phases^{11,14,15,38}.

Sample preparation and analyses. Between 8 and 14 mg of powdered sample was used for each measurement. The powders were pretreated in 30% cold ($\sim 10^\circ\text{C}$) hydrogen peroxide to mitigate potential contamination by organic compounds. Some samples were measured in duplicate to evaluate reproducibility. Sample powders were digested in phosphoric acid at 25 or 90 $^\circ\text{C}$ (Table 1) and analysed following published protocols⁶⁴. The resulting CO_2 was analysed on a customized Thermo MAT 253 gas source mass spectrometer at UCLA dedicated to measuring clumped isotopes in CO_2 . A custom-built, automated, online device⁶⁴ is used to introduce samples to the mass spectrometer.

Isotope data. Values of Δ_{47} are reported as the per mil (‰) difference relative to what would be predicted given a stochastic distribution of isotopes among all possible isotopologues. Values of Δ_{47} are determined by calculating $\delta^{18}\text{O}$, $\delta^{13}\text{C}$, and the abundance of mass-47 isotopologues⁵². This spectrum of masses along with known fractionation factors for $^{18}\text{O}/^{16}\text{O}$ and $^{13}\text{C}/^{12}\text{C}$ allows for quantification of carbonate $\delta^{18}\text{O}$, $\delta^{13}\text{C}$ and Δ_{47} values²⁰. Data are shown in Tables 1 and 2. All Δ_{47} values are reported on the absolute reference frame (ARF), which is calculated using 25 and 1,000 $^\circ\text{C}$ equilibrated gases. These measurements were made before the implementation of a baseline correction scheme.

These Δ_{47} values were converted to temperature using various calibrations^{20,40,41,65–68}. Figures and discussion are based on the calibrations by Tang *et al.*⁴¹ and Tripati *et al.*⁴⁰ and acid fractionation factor of 0.092‰ (ref. 69), which is within error of the value reported by Defliese *et al.*⁶⁵. The acid digestion temperatures, calibrations and fractionation factors yield comparable temperatures (aside from the Dennis and Schrag⁶⁶ calibration, which significantly lower and produces some impossible temperatures). Carbonate $\delta^{13}\text{C}$ and $\delta^{18}\text{O}$ values are reported in ‰ relative to the VPDB standard. The average Δ_{47} precision based on measurements of carbonate standards and samples during the runs for this study

was 0.012‰ (1 s.e.), and select replicate analyses yield an average standard deviation of 0.033‰ (1 s.d.). The average reproducibility of carbonate $\delta^{13}\text{C}$ and $\delta^{18}\text{O}$ are 0.006 and 0.011‰, respectively (Tables 1 and 2).

Data availability. All data pertinent to this manuscript and its reported findings can be found in the manuscript itself or the associated Supplementary Information file.

References

- Childress, J. J. *et al.* A methanotrophic marine mollusc (Bivalvia, Mytilidae) symbiosis: mussels fueled by gas. *Science* **233**, 1306–1308 (1986).
- Reeburgh, W. S. Methane consumption in Cariaco Trench waters and sediments. *Earth Planet. Sci. Lett.* **28**, 337–344 (1976).
- Sassen, R. *et al.* Chemosynthetic bacterial mats at cold hydrocarbon seeps, Gulf of Mexico continental slope. *Org. Geochem.* **20**, 77–89 (1993).
- Orphan, V. J. *et al.* Geological, geochemical, and microbiological heterogeneity of the seafloor around methane vents in the Eel River Basin, offshore California. *Chem. Geol.* **205**, 265–289 (2004).
- Dekas, A. E., Poretsky, R. S. & Orphan, V. J. Deep-sea archaea fix and share nitrogen in methane-consuming microbial consortia. *Science* **326**, 422–426 (2009).
- Valentine, D. L. & Reeburgh, W. S. New perspectives on anaerobic methane oxidation. *Environ. Microbiol.* **2**, 477–484 (2000).
- Raiswell, R. Chemical model for the origin of minor limestone-shale cycles by anaerobic methane oxidation. *Geology* **16**, 641–644 (1988).
- Orphan, V. J., House, C. H., Hinrichs, K. U., McKeegan, K. D. & DeLong, E. F. Multiple archaeal groups mediate methane oxidation in anoxic cold seep sediments. *Proc. Natl Acad. Sci. USA* **99**, 7663–7668 (2002).
- Bohrmann, G. *et al.* Widespread fluid expulsion along the seafloor of the Costa Rica convergent margin. *Terra Nova* **14**, 69–79 (2002).
- Torres, M. E., Martin, R. A., Klinkhammer, G. P. & Nesbitt, E. A. Post depositional alteration of foraminiferal shells in cold seep settings: new insights from flow-through time-resolved analyses of biogenic and inorganic seep carbonates. *Earth. Planet. Sci. Lett.* **299**, 10–22 (2010).
- Joseph, C. *et al.* Methane-derived authigenic carbonates from modern and paleoseeps on the Cascadia margin: mechanisms of formation and diagenetic signals. *Palaeogeogr. Palaeoclimatol. Palaeoecol.* **390**, 52–67 (2013).
- Gieskes, J. *et al.* A study of the chemistry of pore fluids and authigenic carbonates in methane seep environments: Kodiak Trench, Hydrate Ridge, Monterey Bay, and Eel River Basin. *Chem. Geol.* **220**, 329–345 (2005).
- Campbell, K., Farmer, J. & Des Marais, D. Ancient hydrocarbon seeps from the Mesozoic convergent margin of California: carbonate geochemistry, fluids and palaeoenvironments. *Geofluids* **2**, 63–94 (2002).
- Schwartz, H., Sample, J., Weberling, K. D., Minisini, D. & Moore, J. C. An ancient linked fluid migration system: cold-seep deposits and sandstone

- intrusions in the Panoche Hills, California, USA. *Geo-Marine Lett.* **23**, 340–350 (2003).
15. Shapiro, R. & Fricke, H. Tepee buttes. *Fossilized Methane-seep Ecosystems* **3**, 94–101 (2002).
 16. Handa, Y. P. Effect of hydrostatic pressure and salinity on the stability of gas hydrates. *J. Phys. Chem.* **94**, 2652–2657 (1990).
 17. Affek, H. P., Bar-Matthews, M., Ayalon, A., Matthews, A. & Eiler, J. M. Glacial/interglacial temperature variations in Soreq cave speleothems as recorded by ‘clumped isotope’ thermometry. *Geochim. Cosmochim. Acta* **72**, 5351–5360 (2008).
 18. Dennis, K. J., Affek, H. P., Passey, B. H., Schrag, D. P. & Eiler, J. M. Defining an absolute reference frame for ‘clumped’ isotope studies of CO₂. *Geochim. Cosmochim. Acta* **75**, 7117–7131 (2011).
 19. Defliese, W. F. & Lohmann, K. C. Non-linear mixing effects on mass-47 CO₂ clumped isotope thermometry: patterns and implications. *Rapid Commun. Mass Spectrom.* **29**, 901–909 (2015).
 20. Ghosh, P. *et al.* 13 C–18 O bonds in carbonate minerals: a new kind of paleothermometer. *Geochim. Cosmochim. Acta* **70**, 1439–1456 (2006).
 21. Tripathi, A. K. *et al.* 13 C–18 O isotope signatures and ‘clumped isotope’ thermometry in foraminifera and coccoliths. *Geochim. Cosmochim. Acta* **74**, 5697–5717 (2010).
 22. Passey, B. H. & Henkes, G. A. Carbonate clumped isotope bond reordering and geospeedometry. *Earth Planet Sci. Lett.* **351–352**, 223–236 (2012).
 23. Nyman, S. L. & Nelson, C. S. The place of tubular concretions in hydrocarbon cold seep systems: Late Miocene Urenui Formation, Taranaki Basin, New Zealand. *Am. Assoc. Pet. Geol. Bull.* **95**, 1495–1524 (2011).
 24. Suess, E. Marine cold seeps and their manifestations: geological control, biogeochemical criteria and environmental conditions. *Int. J. Earth Sci.* **103**, 1889–1916 (2014).
 25. Hinrichs, K.-U. & Boetius, A. in *Ocean Margin Systems* 457–477 (Springer, 2003).
 26. Barnes, R. & Goldberg, E. Methane production and consumption in anoxic marine sediments. *Geology* **4**, 297–300 (1976).
 27. Bohrmann, G., Greinert, J., Suess, E. & Torres, M. Authigenic carbonates from the Cascadia subduction zone and their relation to gas hydrate stability. *Geology* **26**, 647 (1998).
 28. Kulm, L. *et al.* Oregon subduction zone: venting, fauna, and carbonates. *Science* **231**, 561–566 (1986).
 29. Kulm, L. D. & Suess, E. Relationship between carbonate deposits and fluid venting: Oregon accretionary prism. *J. Geophys. Res. Solid Earth* **95**, 8899–8915 (1990).
 30. Ritger, S., Carson, B. & Suess, E. Methane-derived authigenic carbonates formed by subduction-induced pore-water expulsion along the Oregon/Washington margin. *Geol. Soc. Am. Bull.* **98**, 147–156 (1987).
 31. Burton, E. A. Controls on marine carbonate cement mineralogy: review and reassessment. *Chem. Geol.* **105**, 163–179 (1993).
 32. Greinert, J., Bohrmann, G. & Suess, E. Gas hydrate-associated carbonates and methane-venting at Hydrate Ridge: classification, distribution and origin of authigenic lithologies. *Geophys. Monogr. Am. Geophys. Union* **124**, 99–114 (2001).
 33. Naehr, T. H. *et al.* Authigenic carbonate formation at hydrocarbon seeps in continental margin sediments: a comparative study. *Deep Sea Res. Part II Topical Stud. Oceanogr.* **54**, 1268–1291 (2007).
 34. Schmidt, M. *et al.* Methane hydrate accumulation in “Mound 11” mud volcano, Costa Rica forearc. *Mar. Geol.* **216**, 83–100 (2005).
 35. Hovland, M. & Svensen, H. Submarine pingoos: Indicators of shallow gas hydrates in a pockmark at Nyegga, Norwegian Sea. *Mar. Geol.* **228**, 15–23 (2006).
 36. Mazzini, A., Svensen, H., Hovland, M. & Planke, S. Comparison and implications from strikingly different authigenic carbonates in a Nyegga complex pockmark, G11, Norwegian Sea. *Mar. Geol.* **231**, 89–102 (2006).
 37. Hovland, M. *et al.* Complex pockmarks with carbonate-ridges off mid-Norway: products of sediment degassing. *Mar. Geol.* **218**, 191–206 (2005).
 38. Joseph, C. *et al.* Using the 87Sr/86Sr of modern and paleoseep carbonates from northern Cascadia to link modern fluid flow to the past. *Chem. Geol.* **334**, 122–130 (2012).
 39. Han, X., Suess, E., Sahling, H. & Wallmann, K. Fluid venting activity on the Costa Rica margin: new results from authigenic carbonates. *Int. J. Earth Sci.* **93**, 596–611 (2004).
 40. Tripathi, A. K. *et al.* Beyond temperature: clumped isotope signatures in dissolved inorganic carbon species and the influence of solution chemistry on carbonate mineral composition. *Geochim. Cosmochim. Acta* **166**, 344–371 (2015).
 41. Tang, J., Dietzel, M., Fernandez, A., Tripathi, A. K. & Rosenheim, B. E. Evaluation of kinetic effects on clumped isotope fractionation ($\Delta 47$) during inorganic calcite precipitation. *Geochim. Cosmochim. Acta* **134**, 120–136 (2014).
 42. Nesbitt, E. A., Martin, R. A. & Campbell, K. A. New records of Oligocene diffuse hydrocarbon seeps, northern Cascadia margin. *Palaeogeogr. Palaeoclimatol. Palaeoecol.* **390**, 116–129 (2013).
 43. Kauffman, E. G., Arthur, M. A., Howe, B. & Scholle, P. A. Widespread venting of methane-rich fluids in Late Cretaceous (Campanian) submarine springs (Tepee Buttes), Western Interior seaway, U.S.A. *Geology* **24**, 799 (1996).
 44. Irwin, H., Curtis, C. & Coleman, M. Isotopic evidence for source of diagenetic carbonates formed during burial of organic-rich sediments. *Nature* **269**, 209–213 (1977).
 45. Guo, W., Mosenfelder, J. L., Goddard, W. A. & Eiler, J. M. Isotopic fractionations associated with phosphoric acid digestion of carbonate minerals: Insights from first-principles theoretical modeling and clumped isotope measurements. *Geochim. Cosmochim. Acta* **73**, 7203–7225 (2009).
 46. Thiagarajan, N., Adkins, J. & Eiler, J. Carbonate clumped isotope thermometry of deep-sea corals and implications for vital effects. *Geochim. Cosmochim. Acta* **75**, 4416–4425 (2011).
 47. Tripathi, A., Backman, J., Elderfield, H. & Ferretti, P. Eocene bipolar glaciation associated with global carbon cycle changes. *Nature* **436**, 341–346 (2005).
 48. Zeebe, R. E. & Wolf-Gladrow, D. A. *CO₂ in seawater: equilibrium, kinetics, isotopes* Vol. 65, (Gulf Professional Publishing, 2001).
 49. Hill, P. S., Tripathi, A. K. & Schauble, E. A. Theoretical constraints on the effects of pH, salinity, and temperature on clumped isotope signatures of dissolved inorganic carbon species and precipitating carbonate minerals. *Geochim. Cosmochim. Acta* **125**, 610–652 (2014).
 50. Stakes, D. S., Orange, D., Paduan, J. B., Salamy, K. A. & Maher, N. Cold-seeps and authigenic carbonate formation in Monterey Bay, California. *Mar. Geol.* **159**, 93–109 (1999).
 51. Bristow, T. F., Bonifacie, M., Derkowski, A., Eiler, J. M. & Grotzinger, J. P. A hydrothermal origin for isotopically anomalous cap dolostone cements from south China. *Nature* **474**, 68–71 (2011).
 52. Eiler, J. M. & Schauble, E. 18O13C16O in Earth’s atmosphere. *Geochim. Cosmochim. Acta* **68**, 4767–4777 (2004).
 53. Hong, W.-L., Torres, M. E., Kim, J.-H., Choi, J. & Bahk, J.-J. Carbon cycling within the sulfate-methane-transition-zone in marine sediments from the Ulleung Basin. *Biogeochemistry* **115**, 129–148 (2013).
 54. Brooks, J. M., Field, M. E. & Kennicutt, M. C. Observations of gas hydrates in marine sediments, offshore northern California. *Mar. Geol.* **96**, 103–109 (1991).
 55. Kvenvolden, K. A. & Field, M. E. Thermogenic hydrocarbons in unconsolidated sediment of Eel River Basin, Offshore Northern California: Geologic Notes. *Am. Assoc. Pet. Geol. Bull.* **65**, 1642–1646 (1981).
 56. Torres, M. E. *et al.* Methane sources feeding cold seeps on the shelf and upper continental slope off central Oregon, USA. *Geochem. Geophys. Geosyst.* **10**, 1–21 (2009).
 57. Valentine, D. L., Blanton, D. C., Reeber, W. S. & Kastner, M. Water column methane oxidation adjacent to an area of active hydrate dissociation, Eel River Basin. *Geochim. Cosmochim. Acta* **65**, 2633–2640 (2001).
 58. DePaolo, D. J. Surface kinetic model for isotopic and trace element fractionation during precipitation of calcite from aqueous solutions. *Geochim. Cosmochim. Acta* **75**, 1039–1056 (2011).
 59. Watkins, J. & Hunt, J. A process-based model for non-equilibrium clumped isotope effects in carbonates. *Earth Planet Sci. Lett.* **432**, 152–165 (2015).
 60. Bayon, G., Henderson, G. M. & Bohn, M. U–Th stratigraphy of a cold seep carbonate crust. *Chem. Geol.* **260**, 47–56 (2009).
 61. Omeregie, E. O. *et al.* Biogeochemistry and community composition of iron- and sulfur-precipitating microbial mats at the Chefred mud volcano (Nile Deep Sea Fan, Eastern Mediterranean). *Appl. Environ. Microbiol.* **74**, 3198–3215 (2008).
 62. Aloisi, G., Wallmann, K., Haese, R. R. & Saliège, J. F. Chemical, biological and hydrological controls on the 14C content of cold seep carbonate crusts: numerical modeling and implications for convection at cold seeps. *Chem. Geol.* **213**, 359–383 (2004).
 63. Omeregie, E. O. *et al.* Microbial methane oxidation and sulfate reduction at cold seeps of the deep Eastern Mediterranean Sea. *Mar. Geol.* **261**, 114–127 (2009).
 64. Passey, B. H., Levin, N. E., Cerling, T. E., Brown, F. H. & Eiler, J. M. High-temperature environments of human evolution in East Africa based on bond ordering in paleosol carbonates. *Proc. Natl Acad. Sci.* **107**, 11245–11249 (2010).
 65. Defliese, W. F., Hren, M. T. & Lohmann, K. C. Compositional and temperature effects of phosphoric acid fractionation on $\Delta 47$ analysis and implications for discrepant calibrations. *Chem. Geol.* **396**, 51–60 (2015).
 66. Dennis, K. J. & Schrag, D. P. Clumped isotope thermometry of carbonates as an indicator of diagenetic alteration. *Geochim. Cosmochim. Acta* **74**, 4110–4122 (2010).
 67. Eagle, R. *et al.* The influence of temperature and seawater carbonate saturation state on 13C–18O bond ordering in bivalve mollusks. *Biogeosciences* **10**, 4591–4606 (2013).

68. Zaarur, S., Olack, G. & Affek, H. P. Paleo-environmental implication of clumped isotopes in land snail shells. *Geochim. Cosmochim. Acta* **75**, 6859–6869 (2011).
69. Henkes, G. A. *et al.* Carbonate clumped isotope compositions of modern marine mollusk and brachiopod shells. *Geochim. Cosmochim. Acta* **106**, 307–325 (2013).
70. Henkes, G. A. *et al.* Temperature limits for preservation of primary calcite clumped isotope paleotemperatures. *Geochim. Cosmochim. Acta* **139**, 362–382 (2014).

Acknowledgements

Preliminary discussion and access to some cold seep carbonates provided by Victoria Orphan. Funding for the study was provided to S.L. by the Agouron Geobiology Post-doctoral Fellowship. A.K.T. acknowledges support from the Department of Energy through BES grant DE-FG02-13ER16402.

Author contributions

S.J.L. and A.E.T. conceived study; S.J.L., R.E.T., K.B., L.G.H. and A.E.T. performed analyses; J.S., M.H., M.T., J.M. and T.L. provided samples. All authors contributed to writing the manuscript.

Additional information

Supplementary Information accompanies this paper at <http://www.nature.com/naturecommunications>

Competing financial interests: The authors declare no competing financial interests.

Reprints and permission information is available online at <http://npg.nature.com/reprintsandpermissions/>

How to cite this article: Loyd, S. J. *et al.* Methane seep carbonates yield clumped isotope signatures out of equilibrium with formation temperatures. *Nat. Commun.* **7**:12274 doi: 10.1038/ncomms12274 (2016).



This work is licensed under a Creative Commons Attribution 4.0 International License. The images or other third party material in this article are included in the article's Creative Commons license, unless indicated otherwise in the credit line; if the material is not included under the Creative Commons license, users will need to obtain permission from the license holder to reproduce the material. To view a copy of this license, visit <http://creativecommons.org/licenses/by/4.0/>

© The Author(s) 2016